NUCLEAR THEORY, Vol. 42 (2025)
eds. M. Gaidarov, N. Minkov, Heron Press, Sofia

Beyond-Mean-Field Description of Quadrupole-Hexadecapole Coupling in Atomic Nuclei

R. Rodríguez-Guzmán

Department of Physics, School of Sciencies and Humanities,
Nazarbayev University, 53 Kabanbay Batyr Ave., Astana 010000, Kazakhstan

Abstract. Recent progress in the microscopic understanding of the subtle interplay between the quadrupole and hexadecapole degrees of freedom in atomic nuclei will be discussed, both at the mean-field level and from a (dynamical) beyond-mean-field perspective using the finite range and density dependent Gogny interaction. First, the emergence of (static) hexadecapole deformation effects will be considered within the Hartree-Fock-Bogoliubov (HFB) framework. Second, the stability of those mean-field hexadecapole deformation effects against zero-point quantum fluctuations and their coupling with the quadrupole degree of freedom will be considered within the two-dimensional Generator Coordinate Method (GCM). Results will be illustrated for a large set of even-even Ra, Th, U and Pu isotopes as well as for Yb, Hf, W and Os nuclei. Detailed consideration will be given to static and dynamic features, such as a transition from a regime in which the quadrupole and hexadecapole degrees of freedom are interwoven to a regime in which they are decoupled. It will be shown that, for the studied nuclei, the dynamical quadrupole-hexadecapole configuration mixing brings a nontrivial additional correlation energy gain comparable to the quadrupole correlation energy itself. All these results point towards the non-trivial physics brought by the inclusion of higher order deformations in the dynamics of both ground and excited states.

1 Introduction

The concept of intrinsic deformation plays a prominent role in our understanding of low-energy nuclear structure. Both ground and excited states of atomic nuclei exhibit a broad range of shapes, characterized by the corresponding multiple moments $Q_{\lambda\mu}$ and their associated deformation parameters $\beta_{\lambda\mu}$ [1]. Within this context, axial and triaxial quadrupole deformations, and their impact on spectroscopic nuclear properties, are among the most studied all over the nuclear chart (see, for example, [2–6] and references therein).

Correlation effects associated with octupole deformed shapes have also received close scrutiny (see, for example [7–9] and references therein) in certain regions of the nuclear chart, where those deformations are energetically favored [10]. In particular, previous (constrained) Hartree-Fock-Bogoliubov

(HFB) calculations followed by two-dimensional (2D) Generator Coordinate Method (GCM) calculations [7–9], based on the Gogny [11] energy density functional (EDF), have already revealed a weak coupling between the (axial) quadrupole Q_{20} and octupole Q_{30} moments, a feature that might be anticipated from the different parity quantum numbers of those moments.

In comparison with the quadrupole and octupole cases, higher-order nuclear deformations, such as hexadecapole deformations, have received less detailed attention [12–14]. However, previous Gogny HFB+2D-GCM calculations [14] have revealed the nontrivial effects associated with the inclusion of hexadecapole deformation in the ground state dynamics. It has been found that in some regions of the nuclear chart the quadrupole and hexadecapole degrees of freedom are interwoven, i.e., full-fledged 2D-GCM calculations are required. Furthermore, it has also been shown [14] that 2D-GCM calculations, with the quadrupole β_2 and hexadecapole β_4 parameters as generating coordinates, provide a non trivial additional correlation energy gain comparable to the quadrupole correlation energy itself.

In this contribution, we discuss recent progress [15, 16] in our understanding of the emergence of (static) HFB hexadecapole deformations in different regions of the Segre chart, as well as their stability and coupling to the quadrupole moment once (dynamical) beyond-mean-field correlations are taken into account. The paper is organized as follows. Our theoretical framework, i.e., the HFB+2D-GCM approach [7–9, 15, 16], is briefly outlined in Sec. 2. We have performed calculations for a large set of nuclei in two regions of the nuclear chart, i.e., the isotopic chains $^{232-268}$Ra , $^{232-268}$Th, $^{232-268}$U, $^{232-268}$Pu and the isotopic chains $^{170-202}$Yb, $^{170-202}$Hf, $^{170-202}$W, $^{170-202}$Os. However, in order to illustrate the main tendencies in our calculations as well as for the sake of brevity, in Sec. 3, we will mainly discuss results obtained for U isotopes in the first region, and for W in the second region. We stress that similar results have been obtained for Ra, Th, Pu as well as for Yb, Hf, Os nuclei. Mean-field and beyond-mean-field results will be presented in Secs. 3.1 and 3.2, respectively. Finally, Sec. 4 is devoted to the concluding remarks.

2 Theoretical Framework

We have resorted to the HFB+2D-GCM scheme [7–9, 15, 16]. In what follows, we briefly outline our mean-field and beyond-mean-field computational schemes, based on the parametrization D1S of the Gogny-EDF [11]. First, we have performed Gogny-HFB calculations with (shape) constrains on the axially symmetric quadrupole $\hat{Q}_{20}$ and hexadecapole $\hat{Q}_{40}$ operators. The quadrupole Q_{20} and hexadecapole Q_{40} moments are obtained as average values $Q_{\lambda 0} = \langle\varphi|\hat{Q}_{\lambda 0}|\varphi\rangle$ ($\lambda = 2, 4$) in the HFB states $|\varphi\rangle$. As a result of these constrained calculations, we have obtained the mean-field potential energy surfaces (MFPESs), i.e., the HFB energies as functions of the quadrupole β_2 and hexadecapole β_4

deformations, which are related to the quadrupole Q_{20} and hexadecapole Q_{40} moments as

$$Q_{\lambda 0} = \frac{3R_0^\lambda A}{\sqrt{4\pi(2\lambda+1)}}\beta_\lambda \tag{1}$$

with $R_0 = 1.2A^{1/3}$ and A the mass number. We have employed to a large axially symmetric harmonic oscillator (HO) basis containing 17 major shells with the oscillator lengths $b_\perp = b_z = b_0 = 1.01A^{1/6}$. For each of the studied nuclei, both (intrinsic) HFB states $|\varphi(\vec{\beta})\rangle$ and energies $E_{HFB}(\vec{\beta})$ have been obtained in a large (β_2, β_4)-mesh with appropiate steps $\delta\beta_2$ and $\delta\beta_4$, respectively [15, 16]. Note, that we have introduced the shorthand notation $\vec{\beta} = (\beta_2, \beta_4)$.

As a second step, dynamical fluctuations in the quadrupole and hexadecapole deformations, have been considered in ground ($\sigma = 1$) and excited ($\sigma = 2, 3\cdots$) states with the 2D-GCM ansatz

$$|\Psi^\sigma_{2D-GCM}\rangle = \int d\vec{\beta} f^\sigma(\vec{\beta})|\varphi(\vec{\beta})\rangle \tag{2}$$

where the amplitudes $f^\sigma(\vec{\beta})$ have been determined via the solution of the Griffin-Hill-Wheeler (GHW) equation [1, 15, 16]. As the HFB states $|\varphi(\vec{\beta})\rangle$ are not orthonormal, we need to consider the collective wave functions [1]

$$G^\sigma(\vec{\beta}_1) = \int d\vec{\beta}_2 \, \mathcal{N}^{\frac{1}{2}}(\vec{\beta}_1, \vec{\beta}_2) f^\sigma(\vec{\beta}_2) \tag{3}$$

to obtain a probabilistic interpretation. In Eq. (3) $\mathcal{N}^{\frac{1}{2}}(\vec{\beta}_1, \vec{\beta}_2)$ represents the operational square root of the 2D-GCM norm kernel [1]. Dynamical deformation parameters, associated with the state Eq. (2), can be computed using general expressions developed in previos studies [15, 16].

3 Results

In this section, we discuss the results of calculations. We will mainly concentrate on U and W nuclei, to illustrate the main tendencies in our calculations. Similar results have been obtained for Ra, Th, Pu and Yb, Hf, Os nuclei.

3.1 Results of mean-field calculations

The MFPESs obtained for ^{236,238,240,256,260,268}U and ^{172,176,180,188,192,200}W are depicted in Figures 1 and 2, as illustratives examples. In our calculations for Ra, Th, U and Pu nuclei, we have obtained ground state β_2 values within the range $0.24 \leq \beta_2 \leq 0.28$ up to $A = 248$, whereas for larger mass numbers they decrease reaching values $-0.12 \leq \beta_2 \leq 0.0$ for ^{266,268}Ra, ^{266,268}Th, ^{266,268}U and ^{268}Pu. For $^{170-190}$W the ground state deformations vary within the range $0.18 \leq \beta_2 \leq 0.34$. Oblate-deformed ground states are obtained for $^{192-198}$W

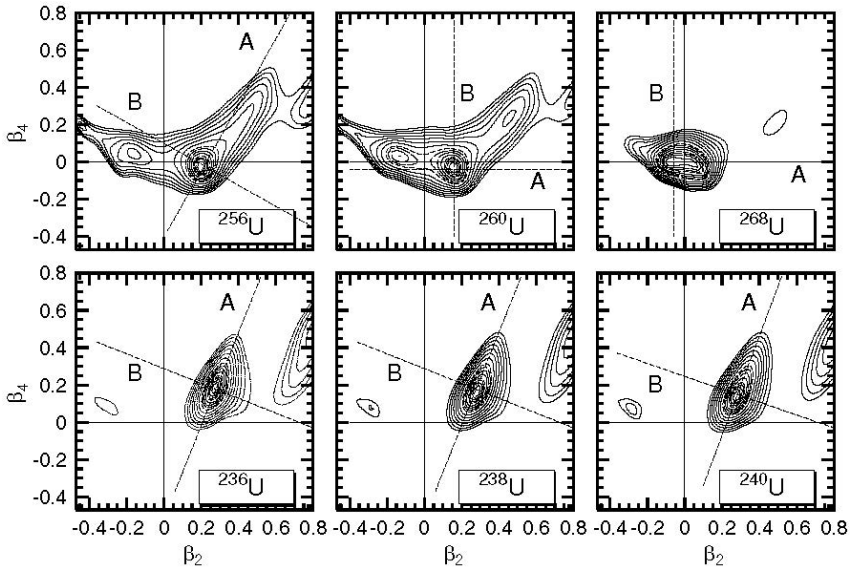

Figure 1. Mean-field potential energy surfaces (MFPESs) computed with the Gogny-D1S energy density functional (EDF) for the isotopes ^{236,238,240,256,260,268}U. Contour lines extend from 0.25 MeV up to 1 MeV above the ground state energy in steps of 0.25 MeV in the ascending sequence full, long-dashed, medium-dashed and short-dashed. The next contours following the same sequence correspond to energies from 1.5 MeV up to 3 MeV above the ground state in steps of 0.5 MeV. From there on, dotted contour lines are drawn in steps of 1 MeV. For each nucleus, the two perpendicular dotted lines A and B are drawn along the principal axes of the parabola that approximates the HFB energy around the absolute minimum of the MFPES. A vertical full line is drawn to signal the $\beta_2 = 0$ line whereas a full horizontal line is drawn to signal the $\beta_4 = 0$ line. For more details, see the main text.

with $-0.16 \leq \beta_2 \leq -0.8$, while $\beta_2 = 0$ for ^{200,202}W. Similar results have been found for $^{170-202}$Yb, $^{170-202}$Hf and $^{170-202}$Os.

As illustrated in Figure 1, sizable HFB β_4 values ($0.09 \leq \beta_2 \leq 0.17$) are obtained around ^{238}U, which agrees well with the conclusions of Ref. [17]. With increasing mass number, the β_4 deformations decrease up to β_4 = 0 for ^{248}Ra, ^{250}Th, ^{252}U and ^{254}Pu. As one approaches the neutron shell closure $N = 184$ [18], negative $-0.04 \leq \beta_4 \leq -0.02$ values are predicted for $^{250-264}$Ra, $^{252-264}$Th, $^{254-264}$U and $^{256-266}$Pu. As can been from Figure 2, diamond-like shapes with $0.04 \leq \beta_4 \leq 0.10$ are found for $^{170-178}$W. On ther other hand, as one approaches the neutron shell closure $N = 126$ [18], negative $-0.08 \leq \beta_4 \leq -0.02$ values are predicted for $^{182-198}$W. The ground states of ^{180,200,202}W correspond to $\beta_4 = 0$. Similar results have been found for Yb, Hf and Os nuclei.

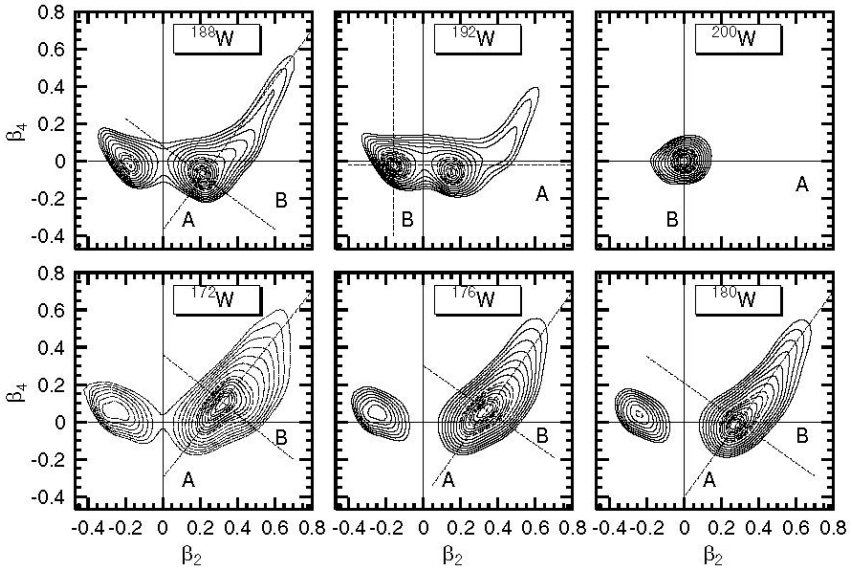

Figure 2. The same as in Figure 1, but for the isotopes ^{172,176,180,188,192,200}W. For more details, see the main text.

In Figures 1 and 2, for each nucleus, the dotted line A runs parallel to the bottom of the energy valley in the neighborhood of the absolute minimum of the MFPES and the line B represents the direction perpendicular to A. Along both directions A and B, the HFB energy exhibits a parabolic behavior and the parameter β_4 depends linearly on β_2 [15, 16]. As can be seen from the figures, for some of the studied nuclei, the lines A and B are tilted with respect to both the β_2 and β_4 axes indicating, that the quadrupole and hexadecapole degrees are interwoven, i.e., full-fledged 2D-GCM calculations must be carried out for those nuclei [15, 16]. On the other hand, in the case of heavier nuclei (such as, for example, ^{260,268}U and ^{192,200}W in the figures) the directions A and B run parallel to the β_2 and β_4 axes, respectively, pointing towards a decoupling of the quadrupole and hexadecapole degrees of freedom. Thus, with increasing mass number, our (static) Gogny-HFB calculations predict a transition from a regime in which the quadrupole and hexadecapole degrees of freedom are interwoven to a regime in which they are decoupled.

3.2 Results of beyond-mean-field calculations

The ground state collective wave functions obtained for ^{236,238,240,256,260,268}U are plotted in Figure 3, as illustrative examples. From a quantum mechanical point of view, the first stricking feature seen from the figure is that for some of the studied nuclei (^{236,238,240,256}U) those collective wave functions align precisely along the directions A and B (see, Figure 1), i.e., the quadrupole and

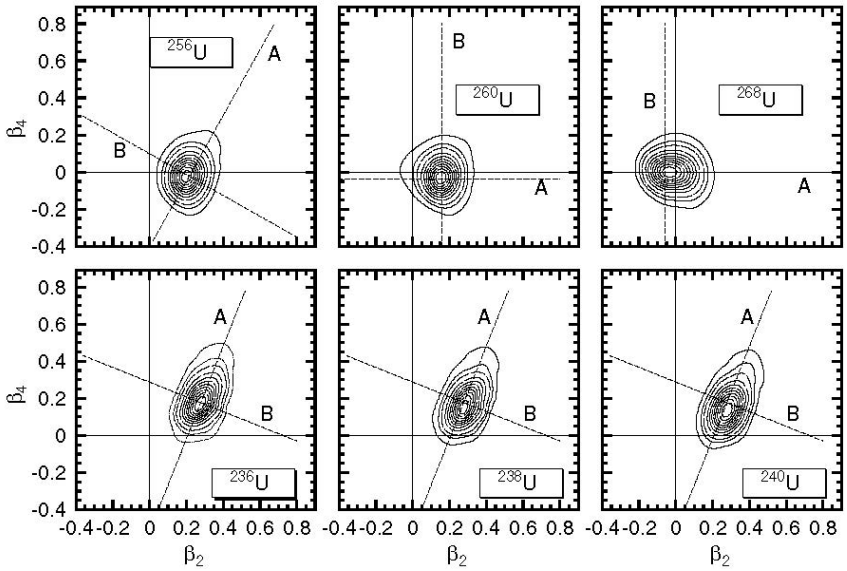

Figure 3. Collective wave functions corresponding to the ground states of the nuclei ^{236,238,240,256,260,268}U. The succession of solid, long dashed and short dashed contour lines starts at 90% of the maximum value up to 10% of it. The two dotted-line contours correspond to the tail of the amplitude (5% and 1% of the maximum value). For each nucleus, the two perpendicular dotted lines A and B are drawn along the principal axes of the parabola that approximates the HFB energy around the absolute minimum of the MFPES and are the same as in Figure 1. A vertical full line is drawn to signal the $\beta_2 = 0$ line whereas a full horizontal line is drawn to signal the $\beta_4 = 0$ line. Results have been obtained with the Gogny-D1S EDF. For more details, see the main text.

hexadecapole degrees are dynamically coupled. On the other hand, for heavier nuclei (^{260,268}U), the strengths align paralell to the β_2 axis, i.e ., the quadrupole-hexadecapole coupling is rather weak.

The collective wave functions corresponding to the first excited states in ^{236,238,240,256,260,268}U are depicted in Figure 4, as illustrative examples. For nuclei such as ^{236,240}U (^{238,256}U) they correspond to phonons aligned along the tilted direction A (B), i.e., the quadrupole and hexadecapole degrees are interwoven. On the other hand, for ^{260,268}U the collective amplitudes align parallel to the quadrupole axis, i.e., the quadrupole and hexadecapole degrees are decupled in those first excited states. Similar conclusions can be extracted from the analysis of the structural evolution of the collective wave functions obtained for $^{232-268}$Ra , $^{232-268}$Th, $^{232-268}$Pu and $^{170-202}$Yb, $^{170-202}$Hf, $^{170-202}$W, $^{170-202}$Os. Thus, for the ground and excited states of the studied nuclei, a transition from a regime in which the quadrupole and hexadecapole degrees of free-

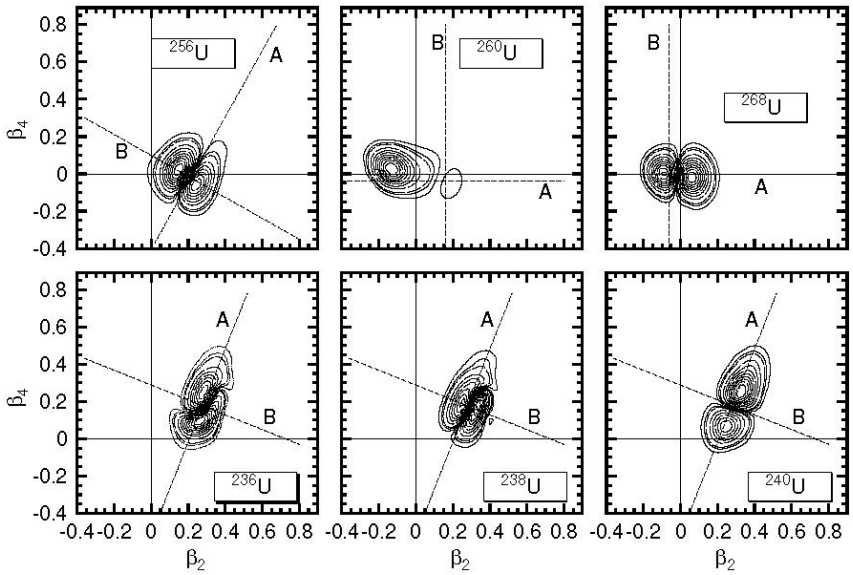

Figure 4. The same as in Figure 3 but for the first excited 2D-GCM states of the nuclei ^{236,238,240,256,260,268}U. For more details, see the main text.

dom are interwoven to a regime in which they are decoupled, takes place with increasing mass number [15, 16].

For ground ($\sigma = 1$) and first excited ($\sigma = 2$) 2D-GCM states, we have computed the corresponding (dynamical) quadrupole and hexadecapole deformations. The values of the ground state $\beta^{\sigma=1}_{2,2D-GCM}$ and $\beta^{\sigma=1}_{4,2D-GCM}$ deformations corroborate the stability of HFB deformation effects. Moreover, in good agreement with the polar gap model [18], the $\beta^{\sigma=1}_{4,2D-GCM}$ values confirm the survival of regions with small negative hexadecapole deformations as we approach the $N = 184$ and $N = 126$ neutron shell closures along the Ra, Th, U, Pu and Yb, Hf, W, Os isotopic chains, respectively. Among other relevant features, the $\beta^{\sigma=2}_{2,2D-GCM}$ and $\beta^{\sigma=2}_{4,2D-GCM}$ deformations obtained for the first excited states reveal, that the transition between different quadrupole-hexadecapole coupling regimes is accompained by an enhanced shape coexistence in the more neutron-rich sectors of the considered isotopic chains. For more details, the reader is referred to Refs. [15, 16].

Finally, let us turn the attention to one of the main outcomes of the calculations. To this end, in Figure 5, we have plotted the 2D-GCM correlation energies $E_{Corr,2D-GCM}$ obtained for $^{232-268}$U and $^{170-202}$W, as illustratives examples. Those correlation energies are defined as the difference

$$E_{Corr,2D-GCM} = E_{HFB,gs} - E^{\sigma=1} \tag{4}$$

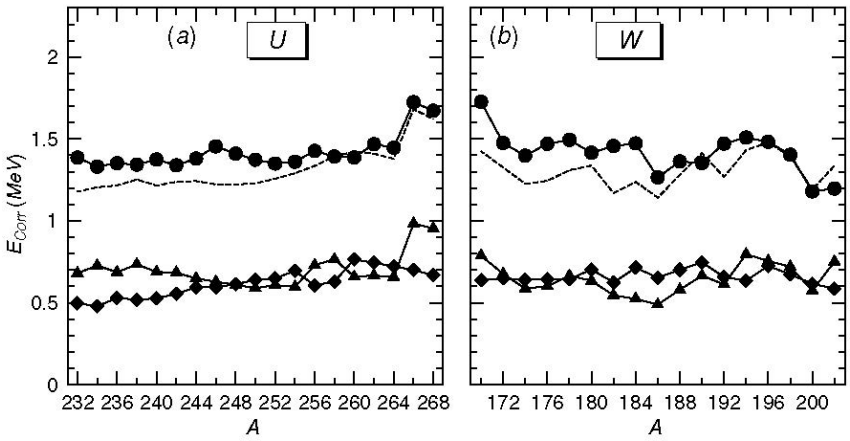

Figure 5. The 2D-GCM correlation energies $E_{Corr,2D-GCM}$ (full circles) obtained for $^{232-268}$U [panel (a)] and $^{170-202}$W [panel (b)]. Correlation energies $E_{Corr,1D-GCM,A}$ and $E_{Corr,1D-GCM,B}$ obtained in 1D-GCM calculations along the directions A (full triangles) and B (full diamonds) are also included in the plots. The dotted lines in the panels correspond to the sum of 1D-GCM correlation energies along the directions A and B. Results have been obtained with the Gogny-D1S EDF. For more details, see the main text.

between the HFB $E_{HFB,gs}$ and 2D-GCM $E^{\sigma=1}$ ground state energies. We have obtained 1.42 MeV $\leq E_{Corr,2D-GCM} \leq 1.72$ MeV and 1.15 MeV $\leq E_{Corr,2D-GCM} \leq 1.73$ MeV for the studied Ra, Th, U, Pu and Yb, Hf, W, Os nuclei, respectively. These ranges of variation (0.30 MeV and 0.58 MeV) compare well with the rms for the binding energy in Gogny mass tables [19], and suggest that $E_{Corr,2D-GCM}$ energies should be included in future parametrizations of the Gogny-EDF.

In Figure 5, we have also included the correlation energies $E_{Corr,1D-GCM,A}$ and $E_{Corr,1D-GCM,B}$ obtained in 1D-GCM calculations along the directions A and B. The figure illustrates the key role of the directions A and B, as the sum $E_{Corr,1D-GCM,A} + E_{Corr,1D-GCM,B}$ accounts for a significant portion of $E_{Corr,2D-GCM}$. Note that, as expected, the energies $E_{Corr,1D-GCM,A}$ are rather similar to the ones obtained in 1D-GCM calculations with the quadrupole moment as single generating coordinate (quadrupole correlation energy) [14–16]. For the studied Ra, Th, U, Pu nuclei we have found that in going from the A and B 1D-GCM to the 2D-GCM calculations, we obtain the additional correlation energies 0.74 MeV $\leq \delta E_{Corr} \leq 0.81$ MeV and 0.66 MeV $\leq \delta E_{Corr} \leq 0.94$ MeV. The corresponding values for Yb, Hf, W, Os nuclei are 0.68 MeV $\leq \delta E_{Corr} \leq 0.77$ MeV and 0.69 MeV $\leq \delta E_{Corr} \leq 0.87$ MeV. These results, represent a warning for GCM practitioners regarding the slow convergence of the

nuclear correlation energy with respect to the shape multipole moments included in the ansatz Eq. (2).

4 Conclusion

In this contribution, we have discussed recent progress in our microscopic understanding of the quadrupole-hexadecapole coupling in atomic nuclei, using the Gogny-D1S HFB+2D-GCM scheme. Results have been discussed for a selected set of Ra, Th, U, Pu and Yb, Hf, W, Os nuclei.

For several of the studied nuclei the MFPESs, obtained at the (static) HFB level, exhibit global minima corresponding to hexadecapole deformations different from zero. At the 2D-GCM level, we have confirmed the stability of mean-field deformation effects as well as the key role played by zero-point (β_2, β_4)-fluctuations in the ground and excited states of the considered nuclei. From a dynamical perspective, the structural evolution of the 2D-GCM collective wave functions corroborates that the ground and excited states of the lighter isotopes, in each of the considered isotopic chains, correspond to diamond-like shapes. On the other hand, square-like shapes have been predicted for Ra, Th, U, Pu and Yb, Hf, W, Os nuclei just below the neutron magic numbers $N = 184$ and $N = 126$, respectively. Furthermore, the patterns observed in the 2D-GCM collective strengths with increasing mass number, point towards a transition from a regime in which the quadrupole and hexadecapole degrees of freedom are interwoven to a regime in which they are decoupled.

For the studied Ra, Th, U, Pu and Yb, Hf, W, Os nuclei, we have found that the ranges of variations of the (β_2, β_4)-GCM correlation energies compare well with the rms for the binding energy in Gogny mass tables. Therefore, such correlation energies should be taken into account in future fitting protocols of the Gogny-EDF. The comparison of 2D-GCM and 1D-GCM calculations, reveals the nontrivial physics brought by the inclusion of hexadecapole deformation in the ground state dynamics. In particular, (β_2, β_4)-GCM calculations provide an additional correlation energy gain similar to the quadrupole correlation energy itself. All these results, encourage a more detailed analysis of the slow convergence of the nuclear correlation energy as well as of the coupling between the quadrupole and higher-order shape multipole moments (for example, hexacontatetrapole β_6 deformations). Work along these lines is in progress and will be reported in future publications.

Acknowledgements

The author acknowledges research funding by Nazarbayev University under Faculty Development Competitive Research Grants Program (FDCRGP) for 2025-2027, Grant 040225FD4712.

References

[1] P. Ring, P. Schuck, *The Nuclear Many-Body Problem* (Springer, Berlin-Heidelberg-New York, 1980).

[2] L.M. Robledo, R. Rodríguez-Guzmán, P. Sarriguren, *J. Phys. G: Nucl. Part. Phys.* **36** (2009) 115104.

[3] R. Rodríguez-Guzmán, P. Sarriguren, L.M. Robledo, J.E. García-Ramos, *Phys. Rev. C* **84** (2010) 024310.

[4] Y. Fu, H. Mei, J. Xiang, Z.P. Li, J.M. Mao, J. Meng, *Phys. Rev. C.* **87** (2013) 054305.

[5] K. Nomura, R. Rodríguez Guzmán, L.M. Robledo, *Phys. Rev. C.* **101** (2020) 014306.

[6] R. Rodríguez-Guzmán, L.M. Robledo, *Phys. Rev. C* **89** (2014) 054310.

[7] R. Rodríguez-Guzmán, Y.M. Humadi, L.M. Robledo, *J. Phys. G: Nucl. Part. Phys.* **48** (2021) 015103.

[8] R. Rodríguez-Guzmán, L.M. Robledo, *Phys. Rev. C* **103** (2021) 044301.

[9] R. Rodríguez-Guzmán, L.M. Robledo, *Phys. Rev. C* **108** (2023) 024301.

[10] P.A. Butler, W. Nazarewicz, *Rev. Mod. Phys.* **68** (1996) 349.

[11] J.F. Berger, M. Girod, D. Gogny, *Nucl. Phys. A* **428** (1984) 23c.

[12] L. Lotina, K. Nomura, *Phys. Rev. C* **109** (2024) 034304.

[13] L. Lotina, K. Nomura, R. Rodríguez-Guzmán, L.M. Robledo, *Phys. Rev. C* **111** (2025) 024301.

[14] C.V. Nithish Kumar, L.M. Robledo, *Phys. Rev. C* **108** (2023) 034312.

[15] R. Rodríguez-Guzmán, L.M. Robledo, *Phys. Rev. C* **111** 024304 (2025) 024304.

[16] R. Rodríguez-Guzmán, L.M. Robledo, *Eur. Phys. J. A* **61** (2025) 166.

[17] W. Ryssens, G. Giacalone, B. Schenke, C. Shen, *Phys. Rev. Lett.* **130** (2023) 212302.

[18] G.-F. Bertsch, *Phys. Lett. B* **26** (1968) 130.

[19] S. Goriely, S. Hilaire, M. Girod, S. Péru, *Phys. Rev. Lett.* **102** (2009) 242501; C. Gonzalez-Boquera, M. Centelles, X. Viñas, L. Robledo, *Phys. Lett. B* **779** (2018) 195.